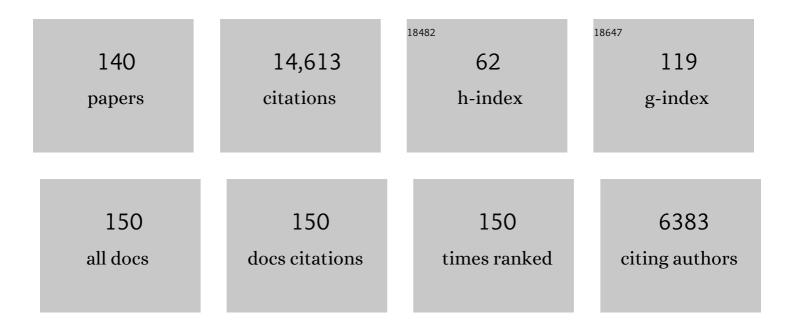
Andrey Bekker

List of Publications by Year in descending order

Source: https://exaly.com/author-pdf/2947423/publications.pdf Version: 2024-02-01



#	Article	IF	CITATIONS
1	Dating the rise of atmospheric oxygen. Nature, 2004, 427, 117-120.	27.8	1,247
2	Tracing the stepwise oxygenation of the Proterozoic ocean. Nature, 2008, 452, 456-459.	27.8	883
3	Iron Formation: The Sedimentary Product of a Complex Interplay among Mantle, Tectonic, Oceanic, and Biospheric Processes. Economic Geology, 2010, 105, 467-508.	3.8	752
4	Iron Isotope Constraints on the Archean and Paleoproterozoic Ocean Redox State. Science, 2005, 307, 1088-1091.	12.6	457
5	Evidence for oxygenic photosynthesis half a billion years before the Great Oxidation Event. Nature Geoscience, 2014, 7, 283-286.	12.9	444
6	Proterozoic ocean redox and biogeochemical stasis. Proceedings of the National Academy of Sciences of the United States of America, 2013, 110, 5357-5362.	7.1	418
7	Widespread iron-rich conditions in the mid-Proterozoic ocean. Nature, 2011, 477, 448-451.	27.8	385
8	Rare Earth Element and yttrium compositions of Archean and Paleoproterozoic Fe formations revisited: New perspectives on the significance and mechanisms of deposition. Geochimica Et Cosmochimica Acta, 2010, 74, 6387-6405.	3.9	373
9	The evolution of the marine phosphate reservoir. Nature, 2010, 467, 1088-1090.	27.8	361
10	Timing and tempo of the Great Oxidation Event. Proceedings of the National Academy of Sciences of the United States of America, 2017, 114, 1811-1816.	7.1	361
11	Iron formations: A global record of Neoarchaean to Palaeoproterozoic environmental history. Earth-Science Reviews, 2017, 172, 140-177.	9.1	304
12	Aerobic bacterial pyrite oxidation and acid rock drainage during the Great Oxidation Event. Nature, 2011, 478, 369-373.	27.8	299
13	Organic-walled microfossils in 3.2-billion-year-old shallow-marine siliciclastic deposits. Nature, 2010, 463, 934-938.	27.8	274
14	Reconstructing Earth's surface oxidation across the Archean-Proterozoic transition. Geology, 2009, 37, 399-402.	4.4	247
15	Large colonial organisms with coordinated growth in oxygenated environments 2.1 Gyr ago. Nature, 2010, 466, 100-104.	27.8	235
16	Suboxic deep seawater in the late Paleoproterozoic: Evidence from hematitic chert and iron formation related to seafloor-hydrothermal sulfide deposits, central Arizona, USA. Earth and Planetary Science Letters, 2007, 255, 243-256.	4.4	228
17	Primitive Os and 2316 Ma age for marine shale: implications for Paleoproterozoic glacial events and the rise of atmospheric oxygen. Earth and Planetary Science Letters, 2004, 225, 43-52.	4.4	225
18	Geological constraints on the origin of oxygenic photosynthesis. Photosynthesis Research, 2011, 107, 11-36.	2.9	200

#	Article	IF	CITATIONS
19	Late Archean to Early Paleoproterozoic global tectonics, environmental change and the rise of atmospheric oxygen. Earth and Planetary Science Letters, 2005, 238, 156-171.	4.4	193
20	Chemostratigraphy of the Paleoproterozoic Duitschland Formation, South Africa: implications for coupled climate change and carbon cycling. Numerische Mathematik, 2001, 301, 261-285.	1.4	188
21	Sulfur record of rising and falling marine oxygen and sulfate levels during the Lomagundi event. Proceedings of the National Academy of Sciences of the United States of America, 2012, 109, 18300-18305.	7.1	174
22	Perspectives on Proterozoic surface ocean redox from iodine contents in ancient and recent carbonate. Earth and Planetary Science Letters, 2017, 463, 159-170.	4.4	172
23	Iron-oxidizing microbial ecosystems thrived in late Paleoproterozoic redox-stratified oceans. Earth and Planetary Science Letters, 2009, 286, 230-242.	4.4	166
24	Titanium isotopic evidence for felsic crust and plate tectonics 3.5 billion years ago. Science, 2017, 357, 1271-1274.	12.6	166
25	Rapid emergence of subaerial landmasses and onset of a modern hydrologic cycle 2.5 billion years ago. Nature, 2018, 557, 545-548.	27.8	153
26	Atmospheric Sulfur in Archean Komatiite-Hosted Nickel Deposits. Science, 2009, 326, 1086-1089.	12.6	152
27	Iron isotope composition of some Archean and Proterozoic iron formations. Geochimica Et Cosmochimica Acta, 2012, 80, 158-169.	3.9	147
28	Triple oxygen isotope evidence for limited mid-Proterozoic primary productivity. Nature, 2018, 559, 613-616.	27.8	144
29	Chemostratigraphy of Paleoproterozoic carbonate successions of the Wyoming Craton: tectonic forcing of biogeochemical change?. Precambrian Research, 2003, 120, 279-325.	2.7	136
30	Trace elements at the intersection of marine biological and geochemical evolution. Earth-Science Reviews, 2016, 163, 323-348.	9.1	135
31	Carbon isotope record for the onset of the Lomagundi carbon isotope excursion in the Great Lakes area, North America. Precambrian Research, 2006, 148, 145-180.	2.7	132
32	Correlation of Paleoproterozoic glaciations based on U–Pb zircon ages for tuff beds in the Transvaal and Huronian Supergroups. Earth and Planetary Science Letters, 2013, 382, 173-180.	4.4	132
33	Evidence for Paleoproterozoic cap carbonates in North America. Precambrian Research, 2005, 137, 167-206.	2.7	127
34	Pyrite multiple-sulfur isotope evidence for rapid expansion and contraction of the early Paleoproterozoic seawater sulfate reservoir. Earth and Planetary Science Letters, 2014, 389, 95-104.	4.4	118
35	Rise in seawater sulphate concentration associated with the Paleoproterozoic positive carbon isotope excursion: evidence from sulphate evaporites in the â^¼2.2–2.1 Gyr shallowâ€marine Lucknow Formation, South Africa. Terra Nova, 2008, 20, 108-117.	2.1	114
36	Onset of the aerobic nitrogen cycle during the Great Oxidation Event. Nature, 2017, 542, 465-467.	27.8	114

#	Article	IF	CITATIONS
37	Multiple sulphur and iron isotope composition of detrital pyrite in Archaean sedimentary rocks: A new tool for provenance analysis. Earth and Planetary Science Letters, 2009, 286, 436-445.	4.4	113
38	Deposition of 1.88-billion-year-old iron formations as a consequence of rapid crustal growth. Nature, 2012, 484, 498-501.	27.8	112
39	The chlorine isotope composition of chondrites and Earth. Geochimica Et Cosmochimica Acta, 2013, 107, 189-204.	3.9	112
40	An iodine record of Paleoproterozoic surface ocean oxygenation. Geology, 2014, 42, 619-622.	4.4	111
41	A 200-million-year delay in permanent atmospheric oxygenation. Nature, 2021, 592, 232-236.	27.8	105
42	Claypool continued: Extending the isotopic record of sedimentary sulfate. Chemical Geology, 2019, 513, 200-225.	3.3	102
43	Fractionation between inorganic and organic carbon during the Lomagundi (2.22–2.1ÂGa) carbon isotope excursion. Earth and Planetary Science Letters, 2008, 271, 278-291.	4.4	96
44	Cobalt and marine redox evolution. Earth and Planetary Science Letters, 2014, 390, 253-263.	4.4	95
45	Fungus-like mycelial fossils in 2.4-billion-year-old vesicular basalt. Nature Ecology and Evolution, 2017, 1, 141.	7.8	94
46	Nickel Isotope Variations in Terrestrial Silicate Rocks and Geological Reference Materials Measured by <scp>MC</scp> â€ <scp>ICP</scp> â€ <scp>MS</scp> . Geostandards and Geoanalytical Research, 2013, 37, 297-317.	3.1	91
47	Uranium in iron formations and the rise of atmospheric oxygen. Chemical Geology, 2013, 362, 82-90.	3.3	91
48	Late Archean euxinic conditions before the rise of atmospheric oxygen. Geology, 2011, 39, 119-122.	4.4	87
49	District to Camp Controls on the Genesis of Komatiite-Hosted Nickel Sulfide Deposits, Agnew-Wiluna Greenstone Belt, Western Australia: Insights from the Multiple Sulfur Isotopes. Economic Geology, 2012, 107, 781-796.	3.8	86
50	Coupled Fe and S isotope variations in pyrite nodules from Archean shale. Earth and Planetary Science Letters, 2014, 392, 67-79.	4.4	86
51	Chemostratigraphy of Carbonates from the Minas Supergroup, Quadrilatero Ferryifero (Iron) Tj ETQq1 1 0.784314 Climactic Change. Numerische Mathematik, 2003, 303, 865-904.	4 rgBT /Ον 1.4	erlock 10 85
52	Biological carbon precursor to diagenetic siderite with spherical structures in iron formations. Nature Communications, 2013, 4, 1741.	12.8	85
53	Bioavailability of zinc in marine systems through time. Nature Geoscience, 2013, 6, 125-128.	12.9	84
54	The geologic history of seawater oxygen isotopes from marine iron oxides. Science, 2019, 365, 469-473.	12.6	81

#	Article	IF	CITATIONS
55	Oxidative forcing of global climate change: A biogeochemical record across the oldest Paleoproterozoic ice age in North America. Earth and Planetary Science Letters, 2007, 258, 486-499.	4.4	79
56	Filling in the juvenile magmatic gap: Evidence for uninterrupted Paleoproterozoic plate tectonics. Earth and Planetary Science Letters, 2014, 388, 123-133.	4.4	79
57	Seafloor-hydrothermal Si-Fe-Mn exhalites in the Pecos greenstone belt, New Mexico, and the redox state of ca. 1720 Ma deep seawater. , 2009, 5, 302-314.		78
58	Evidence for episodic oxygenation in a weakly redox-buffered deep mid-Proterozoic ocean. Chemical Geology, 2018, 483, 581-594.	3.3	73
59	Controls of eustasy and diagenesis on the 238U/235U of carbonates and evolution of the seawater (234U/238U) during the last 1.4 Myr. Geochimica Et Cosmochimica Acta, 2018, 242, 233-265.	3.9	73
60	Multiple Sulfur and Iron Isotope Composition of Magmatic Ni-Cu-(PGE) Sulfide Mineralization from Eastern Botswana. Economic Geology, 2012, 107, 105-116.	3.8	71
61	Pervasive aerobic nitrogen cycling in the surface ocean across the Paleoproterozoic Era. Earth and Planetary Science Letters, 2018, 500, 117-126.	4.4	70
62	Selenium isotopes record extensive marine suboxia during the Great Oxidation Event. Proceedings of the United States of America, 2017, 114, 875-880.	7.1	67
63	A model for the oceanic mass balance of rhenium and implications for the extent of Proterozoic ocean anoxia. Geochimica Et Cosmochimica Acta, 2018, 227, 75-95.	3.9	66
64	Oxygen isotope perspective on crustal evolution on early Earth: A record of Precambrian shales with emphasis on Paleoproterozoic glaciations and Great Oxygenation Event. Earth and Planetary Science Letters, 2016, 437, 101-113.	4.4	62
65	Global nature of the Paleoproterozoic Lomagundi carbon isotope excursion: A review of occurrences in Brazil, India, and Uruguay. Precambrian Research, 2010, 182, 274-299.	2.7	61
66	Needs and opportunities in mineral evolution research. American Mineralogist, 2011, 96, 953-963.	1.9	61
67	Unradiogenic strontium and moderate-amplitude carbon isotope variations in early Tonian seawater after the assembly of Rodinia and before the Bitter Springs Excursion. Precambrian Research, 2017, 298, 157-173.	2.7	60
68	The evolution of the global selenium cycle: Secular trends in Se isotopes and abundances. Geochimica Et Cosmochimica Acta, 2015, 162, 109-125.	3.9	59
69	Chemostratigraphy of the Shaler Supergroup, Victoria Island, NW Canada: A record of ocean composition prior to the Cryogenian glaciations. Precambrian Research, 2015, 263, 232-245.	2.7	59
70	Two-step deoxygenation at the end of the Paleoproterozoic Lomagundi Event. Earth and Planetary Science Letters, 2018, 486, 70-83.	4.4	58
71	A Paleoproterozoic drowned carbonate platform on the southeastern margin of the Wyoming Craton: a record of the Kenorland breakup. Precambrian Research, 2003, 120, 327-364.	2.7	56
72	Nitrogen cycle in the Late Archean ferruginous ocean. Chemical Geology, 2013, 362, 115-130.	3.3	56

#	Article	IF	CITATIONS
73	Comparing orthomagmatic and hydrothermal mineralization models for komatiite-hosted nickel deposits in Zimbabwe using multiple-sulfur, iron, and nickel isotope data. Mineralium Deposita, 2014, 49, 75-100.	4.1	56
74	Aerobic iron and manganese cycling in a redox-stratified Mesoarchean epicontinental sea. Earth and Planetary Science Letters, 2018, 500, 28-40.	4.4	54
75	The 2.1 Ga Old Francevillian Biota: Biogenicity, Taphonomy and Biodiversity. PLoS ONE, 2014, 9, e99438.	2.5	53
76	Re–Os depositional age for Archean carbonaceous slates from the southwestern Superior Province: Challenges and insights. Earth and Planetary Science Letters, 2009, 280, 83-92.	4.4	52
77	Ediacara biota flourished in oligotrophic and bacterially dominated marine environments across Baltica. Nature Communications, 2018, 9, 1807.	12.8	48
78	A persistently low level of atmospheric oxygen in Earth's middle age. Nature Communications, 2021, 12, 351.	12.8	48
79	Organism motility in an oxygenated shallow-marine environment 2.1 billion years ago. Proceedings of the United States of America, 2019, 116, 3431-3436.	7.1	47
80	A review of the stratigraphy and geological setting of the Palaeoproterozoic Magondi Supergroup, Zimbabwe – Type locality for the Lomagundi carbon isotope excursion. Precambrian Research, 2010, 182, 254-273.	2.7	44
81	Microbe-clay interactions as a mechanism for the preservation of organic matter and trace metal biosignatures in black shales. Chemical Geology, 2017, 459, 75-90.	3.3	42
82	Limited oxygen production in the Mesoarchean ocean. Proceedings of the National Academy of Sciences of the United States of America, 2019, 116, 6647-6652.	7.1	42
83	The Archean komatiite-hosted, PGE-bearing Ni–Cu sulfide deposit at Vaara, eastern Finland: evidence for assimilation of external sulfur and post-depositional desulfurization. Mineralium Deposita, 2013, 48, 967-989.	4.1	38
84	Correlation of the stratigraphic cover of the Pilbara and Kaapvaal cratons recording the lead up to Paleoproterozoic Icehouse and the GOE. Earth-Science Reviews, 2020, 211, 103389.	9.1	34
85	Shallow water anoxia in the Mesoproterozoic ocean: Evidence from the Bashkir Meganticlinorium, Southern Urals. Precambrian Research, 2018, 317, 196-210.	2.7	32
86	U–Th–Pb–REE systematics of organic-rich shales from the ca. 2.15ÂGa Sengoma Argillite Formation, Botswana: Evidence for oxidative continental weathering during the Great Oxidation Event. Chemical Geology, 2009, 260, 172-185.	3.3	31
87	Exceptional preservation of expandable clay minerals in the ca. 2.1Ga black shales of the Francevillian basin, Gabon and its implication for atmospheric oxygen accumulation. Chemical Geology, 2013, 362, 181-192.	3.3	31
88	Molybdenum record from black shales indicates oscillating atmospheric oxygen levels in the early Paleoproterozoic. Numerische Mathematik, 2018, 318, 275-299.	1.4	31
89	Development of Iron Speciation Reference Materials for Palaeoredox Analysis. Geostandards and Geoanalytical Research, 2020, 44, 581-591.	3.1	31
90	The Role of Paragneiss Assimilation in the Origin of the Voisey's Bay Ni-Cu Sulfide Deposit, Labrador: Multiple S and Fe Isotope Evidence. Economic Geology, 2013, 108, 1459-1469.	3.8	30

#	Article	IF	CITATIONS
91	The uranium isotopic record of shales and carbonates through geologic time. Geochimica Et Cosmochimica Acta, 2021, 300, 164-191.	3.9	28
92	Sedimentological and geochemical basin analysis of the Paleoproterozoic Penrhyn and Piling groups of Arctic Canada. Precambrian Research, 2014, 251, 80-101.	2.7	26
93	A short-term, post-Lomagundi positive C isotope excursion at <i>c.</i> 2.03â€Ca recorded by the Wooly Dolomite, Western Australia. Journal of the Geological Society, 2016, 173, 689-700.	2.1	26
94	Earth's Great Oxidation Event facilitated by the rise of sedimentary phosphorus recycling. Nature Geoscience, 2022, 15, 210-215.	12.9	26
95	Revised stratigraphic framework for the lower Anti-Atlas Supergroup based on U–Pb geochronology of magmatic and detrital zircons (Zenaga and Bou Azzer-El Graara inliers, Anti-Atlas Belt, Morocco). Journal of African Earth Sciences, 2020, 171, 103946.	2.0	23
96	A late Paleoproterozoic (1.74ÂGa) deepâ€sea, lowâ€temperature, ironâ€oxidizing microbial hydrothermal vent community from Arizona, USA. Geobiology, 2021, 19, 228-249.	2.4	22
97	Geochemistry of pyrite from diamictites of the Boolgeeda Iron Formation, Western Australia with implications for the GOE and Paleoproterozoic ice ages. Chemical Geology, 2013, 362, 131-142.	3.3	19
98	Triple iron isotope constraints on the role of ocean iron sinks in early atmospheric oxygenation. Science, 2020, 370, 446-449.	12.6	19
99	Atmospheric S and lithospheric Pb in sulphides from the 2.06 Ga Phalaborwa phoscorite-carbonatite Complex, South Africa. Earth and Planetary Science Letters, 2020, 530, 115939.	4.4	18
100	A template for an improved rock-based subdivision of the pre-Cryogenian timescale. Journal of the Geological Society, 2022, 179, .	2.1	18
101	Chemostratigraphic constraints on early Ediacaran carbonate ramp dynamics, RÃo de la Plata craton, Uruguay. Gondwana Research, 2012, 22, 1073-1090.	6.0	17
102	Microbially induced potassium enrichment in Paleoproterozoic shales and implications for reverse weathering on early Earth. Nature Communications, 2019, 10, 2670.	12.8	17
103	Long-term evolution of terrestrial weathering and its link to Earth's oxygenation. Earth and Planetary Science Letters, 2022, 584, 117490.	4.4	17
104	Early history of the Amadeus Basin: Implications for the existence and geometry of the Centralian Superbasin. Precambrian Research, 2015, 259, 232-242.	2.7	15
105	Elemental geochemistry and Nd isotope constraints on the provenance of the basal siliciclastic succession of the middle Paleoproterozoic Francevillian Group, Gabon. Precambrian Research, 2020, 348, 105874.	2.7	15
106	Provenance of metasiliciclastic rocks at the northwestern margin of the East Gabonian Block: Implications for deposition of BIFs and crustal evolution in southwestern Cameroon. Precambrian Research, 2022, 376, 106677.	2.7	15
107	Stratigraphy of the Late Palaeoproterozoic (â^¼2.03 Ga) Wooly Dolomite, Ashburton Province, Western Australia: A carbonate platform developed in a failed rift basin. Precambrian Research, 2015, 271, 1-19.	2.7	14
108	Reply to comment on "Bekker, A., Krapež, B., Karhu, J.A., 2020. Correlation of the stratigraphic cover of the Pilbara and Kaapvaal cratons recording the lead up to Paleoproterozoic Icehouse and the GOE. Earth-Science Reviews, 211, 103,389―by Pascal Philippot, Bryan A. Killingsworth, Jean-Louis Paquette, Svetlana Tessalina, Pierre Cartigny, Stefan V. Lalonde, Christophe Thomazo, Janaina N. Ãvila, Vincent Busigny. Earth-Science Reviews, 2021, 218, 103607.	9.1	13

#	Article	IF	CITATIONS
109	Mass-independently fractionated sulfur in Archean paleosols: A large reservoir of negative Δ33S anomaly on the early Earth. Chemical Geology, 2013, 362, 74-81.	3.3	12
110	Postâ€Great Oxidation Event Orosirian–Statherian iron formations on the São Francisco craton: Geotectonic implications. Island Arc, 2019, 28, e12300.	1.1	12
111	Anoxic continental surface weathering recorded by the 2.95â€ ⁻ Ga Denny Dalton Paleosol (Pongola) Tj ETQq1 1	0.784314	rgBT /Overlo
112	The early Statherian (ca. 1800–1750ÂMa) Prutivka-Novogol large igneous province of Sarmatia: Geochronology and implication for the Nuna/Columbia supercontinent reconstruction. Precambrian Research, 2021, 358, 106185.	2.7	11
113	Transient deep-water oxygenation recorded by rare Mesoproterozoic phosphorites, South Urals. Precambrian Research, 2021, 360, 106242.	2.7	9
114	Earth's oldest preserved K-bentonites in the <i>ca</i> . 2.1 Ga Francevillian Basin, Gabon. Numerische Mathematik, 2018, 318, 409-434.	1.4	8
115	Diagenetic history of the proterozoic carbonates and its role in the oil field development in the Baikit Anteclise, Southwestern Siberia. Precambrian Research, 2020, 342, 105690.	2.7	7
116	Oxygen production and rapid iron oxidation in stromatolites immediately predating the Great Oxidation Event. Earth and Planetary Science Letters, 2022, 582, 117416.	4.4	7
117	Paleoproterozoic high δ13Ccarb marbles from the Ruwenzori Mountains, Uganda: Implications for the age of the Buganda Group. Chemical Geology, 2013, 362, 157-164.	3.3	6
118	Constraining provenance for the uraniferous Paleoproterozoic Francevillian Group sediments (Gabon) with detrital zircon geochronology and geochemistry. Precambrian Research, 2020, 343, 105724.	2.7	6
119	Mesoarchaean acidic volcanic lakes: A critical ecological niche in early land colonisation. Earth and Planetary Science Letters, 2021, 556, 116725.	4.4	6
120	Lomagundi Carbon Isotope Excursion. , 2014, , 1-6.		6
121	The Black Angel deposit, Greenland: a Paleoproterozoic evaporite-related Mississippi Valley-type Zn–Pb deposit. Mineralium Deposita, 2023, 58, 51-73.	4.1	6
122	Evolution of the atmosphere and ocean through time. Chemical Geology, 2013, 362, 1-2.	3.3	5
123	Preservation and Distributions of Covalently Bound Polyaromatic Hydrocarbons in Ancient Biogenic Kerogens and Insoluble Organic Macromolecules. Astrobiology, 2021, 21, 1049-1075.	3.0	5
124	Great Oxygenation Event. , 2014, , 1-9.		4
125	Great Oxygenation Event. , 2015, , 1009-1017.		4
126	Lomagundi Carbon Isotope Excursion. , 2015, , 1399-1404.		4

#	ARTICLE	IF	CITATIONS
127	Archean-Proterozoic unconformity on the Fennoscandian Shield: Geochemistry and Sr, C and O isotope composition of Paleoproterozoic carbonate-rich regolith from Segozero Lake (Russian) Tj ETQq1 1 0.78	43 1247rgB1	- O4erlock 10
128	Reply to the comment by $Pr\tilde{A}$ ©at and Weber on. Earth and Planetary Science Letters, 2019, 511, 259-261.	4.4	3
129	Trace element perspective into the ca. 2.1-billion-year-old shallow-marine microbial mats from the Francevillian Group, Gabon. Chemical Geology, 2020, 543, 119620.	3.3	3
130	Ironstones and Iron Formations. , 2021, , 914-921.		3
131	Discussion on â€~From Pan-African transpression to Cadomian transtension at the West African margin: new U–Pb zircon ages from the Eastern Saghro Inlier (Anti-Atlas, Morocco)' by Errami <i>et al</i> . 2020 (<i>SP</i> 503, 209–233). Journal of the Geological Society, 2021, 178, .	2.1	3
132	Limited expression of the Paleoproterozoic Oklo natural nuclear reactor phenomenon in the aftermath of a widespread deoxygenation event ~2.11–2.06 billion years ago. Chemical Geology, 2021, 578, 120315.	3.3	3
133	Huronian Glaciation. , 2014, , 1-8.		3
134	Reply to Comment by C. Gaucher et al. on "Chemostratigraphic constraints on early Ediacaran carbonate ramp dynamics, RÃo de la Plata craton, Uruguay" by Aubet et al. Gondwana Research (2012), Volume 22, Issues 3-4, November 2012, Pages 1073-1090. Gondwana Research, 2013, 23, 1186-1188.	6.0	2
135	Benthic redox conditions and nutrient dynamics in the ca. 2.1ÂGa Franceville sub-basin. Precambrian Research, 2021, 360, 106234.	2.7	2
136	Insights from modern diffuse-flow hydrothermal systems into the origin of post-GOE deep-water Fe-Si precipitates. Geochimica Et Cosmochimica Acta, 2022, 317, 1-17.	3.9	2
137	Huronian Glaciation. , 2015, , 1128-1135.		2
138	Carbon Isotopes in the Solar System. , 2020, , 1-10.		1
139	Lomagundi Carbon Isotope Excursion. , 2022, , 1-7.		1
140	The Timing of the Palaeoproterozoic Great Oxidation Event using Dykes, Sills and Bolcanics of the Ongeluk Large Igneous Province, Kaapvaal Craton. Acta Geologica Sinica, 2016, 90, 67-68.	1.4	0